



# Efficient numerical implementation of limit equilibrium method for stability analysis of unsaturated soil slopes using Gaussian integral

Weihang Ouyang<sup>1</sup> · Siwei Liu<sup>1</sup> · Kai Liu<sup>1</sup> · Jianhua Yin<sup>1</sup>

Received: 4 July 2023 / Accepted: 16 January 2024  
© The Author(s) 2024

## Abstract

Unsaturated soil is widely distributed around the world but less considered in design due to the absence of a convenient analysis method in practice. The Morgenstern–Price (MP) method incorporating the extended Mohr–Coulomb shear strength equation provides a reliable approach to evaluate slope stability in such conditions. However, this method is time-consuming due to the need for a tedious trial-and-error process in determining the scaling factor, which involves complex iterations during each trial. Furthermore, since the relatively complicated nature of unsaturated soil, a dense slice division is necessary to obtain reliable results, making the analysis even more cumbersome. In this paper, an improved MP method for unsaturated soil slope stability analysis is presented, which eliminates the need for a dense slice mesh by employing only a few strategically placed Gauss points along the slip surface. Moreover, the trial-and-error process for determining the scaling factor with the corresponding complex iterations is replaced by an efficient search algorithm with a more concise iteration process, resulting in a more convenient implementation of the proposed method. Extensive examples are provided to validate the effectiveness of the proposed improved MP method, indicating its potential as an accurate and efficient analysis method for unsaturated soil slopes in practical application and relative study involving repetitive analyses.

**Keywords** Gaussian integral · Morgenstern–Price method · Numerical implementation · Slope stability analysis · Unsaturated soil slopes

## 1 Introduction

Unsaturated soil slopes present a critical concern in geotechnical engineering due to the significant reduction in soil shear strength caused by water infiltration [2, 4, 19, 24, 31, 37]. Such strength reduction can cause severe failures in both natural and man-made slopes, especially for those in reservoir areas, such as more than 60

landslides occurred in the Three Gorges Reservoir region since 2003 [39]. The primary triggers for these landslides are repeated water infiltration due to rainfall and fluctuating reservoir water levels, leading to significant damage to both human life and engineering structures. Although analyzing slope stability based on saturated soil mechanics might appear as an approach to prevent such catastrophic events, it sometimes results in excessively conservative and inefficient design outcomes, imposing substantial construction costs for large-scale geotechnical projects [9, 15, 40, 42]. Thus, the feature of unsaturated soil slope must be appropriately evaluated for a safe and economical design result. However, the investigations of slope stability in design are mainly performed on slopes under saturated or dry conditions due to the lack of suitable analysis methods in practice [22].

Various methods have been developed for slope stability analysis over the past few decades, including limit analysis method (LAM) [34], finite element method (FEM) [4, 7, 13, 16, 27, 46], and limit equilibrium method (LEM) [12, 43–45]. The LAM is usually used in simple

---

✉ Kai Liu  
kevin.kai.liu@hotmail.com; kevin-kai.liu@connect.polyu.hk

Weihang Ouyang  
weihang.ouyang@connect.polyu.hk

Siwei Liu  
si-wei.liu@polyu.edu.hk

Jianhua Yin  
cejhyin@polyu.edu.hk

<sup>1</sup> Department of Civil and Environmental Engineering, The Hong Kong Polytechnic University, Hung Hom, Kowloon, Hong Kong, China

geotechnical problems but less suitable for complicated geological conditions in engineering practice. For more general slope stability analysis methods, the FEM has been employed to evaluate the slope stability by incorporating the strength reduction technique. This method is robust; however, it requires solid knowledge of constitutive models, linear and nonlinear failure criteria, and plasticity flow rules for determining critical slip surfaces [6, 20, 26]. In addition, the effort and cost of FEM are sometimes unbearable in design practice [8, 21]. Consequently, the LEM is still the predominant slope stability analysis method in current design practice and recommended by various specifications [1, 38].

In the conventional LEM, the potential sliding soil mass is required to be discretized as vertical slices. The factor of safety (FOS) is calculated based on the force and moment equilibrium of the potential sliding soil mass. Different methods have been proposed based on various assumptions of interslice forces and satisfied conditions for force and moment equilibrium, including Bishop method [3], Morgenstern–Price (MP) method [23], Spencer method [33], Sarma method [28], and Janbu method [17]. Among these methods, the MP method is the most widely used approach since it satisfies stricter equilibrium conditions [26, 48]. Subsequently, various shear strength equations, such as the extended Mohr–Coulomb shear strength equation [11], have been introduced in this method to extend it from only saturated/dry soil slopes to those unsaturated. However, this MP method is still less employed for the unsaturated slope stability analysis in design practices since it is relatively time-consuming and complicated in implementation.

In the MP method, the ratio of normal to shear interslice forces is assumed to be related to a scaling factor,  $\lambda$ , which is determined through the best-fit method [12]. In this best-fit method, multiple trial factors are generated, among which the one that can simultaneously satisfy both force and moment equilibrium conditions of soil slices will be selected as the scaling factor. This best-fit method for  $\lambda$  is robust; however, it can lead to a time-consuming searching procedure since numbers of trial factors might be employed. Additionally, to determine whether two equilibrium conditions are satisfied, the FOSs for both equilibrium conditions with different trial factors must be obtained through a complicated iteration process, which involves initializing interslice force distribution and also repeatedly updating numbers of slice variables, as shown in Fig. 1a. Moreover, since the distributed forces along the slip surface are more complex due to matric suction, a dense slice division, sometimes more than 100 slices [48], is required to obtain reliable results, rendering the iteration procedure more tedious. All of these reasons make the implementation of this analysis method for unsaturated soil slopes complicated and time-consuming, limiting its

application in design practice and some related research that involves repetitive slope stability analyses, such as reliability assessments [21].

In this study, an efficient numerical implementation of the LEM for stability analysis of unsaturated soil slopes is presented. An improved MP method proposed by Ouyang et al. [26] for dry slopes is extended to evaluate the stability of unsaturated soil slopes, where the dense division of slice is replaced by the alignment of only several Gauss points. To improve the searching efficiency of the scaling factor, a linear search method is introduced to replace the best-fit method. Moreover, this paper firstly proposes a refined iteration process for the FOS with the given scaling factor (as shown in Fig. 1b), making the implementation process of the improved MP method for unsaturated slopes more convenient and efficient. To validate the robustness and efficiency of the proposed method, two benchmark examples are provided, including homogeneous and nonhomogeneous unsaturated soil slopes. Finally, two case studies of unsaturated residual soil slopes in Hong Kong are illustrated for future applications in engineering practice. It is believed that this improved MP method for unsaturated slopes will be a useful tool for investigating the unsaturated feature of slope stability in design practice.

## 2 Assumptions

There are some assumptions in this study for evaluating the slope stability of unsaturated soil slopes: (a) resisting forces on the slip surface are computed via the extended Mohr–Coulomb theory; (b) the distribution of the directions of interslice forces can be described using a continuous function; (c) the shape of the slip surface is expressed via a polyline with points or a circular shape; (d) the slope is not strengthened by soil nails, retaining walls, or other constructed elements; (e) the negative water pressure in soil pores is considered; and (f) the gravity load of soils is considered, while other external loads on the slope are not considered.

## 3 The Morgenstern–Price method for unsaturated soil slopes

The Morgenstern–Price (MP) method is a preferable LEM analysis method that originally proposed by Morgenstern and Price [23] for evaluating the stability of the saturated slope. This MP method is extensively recommended in specifications because it considers a rigorous equilibrium condition, which means that both force and moment equilibrium conditions are satisfied. For extending this method to the unsaturated slope, an equation for shear

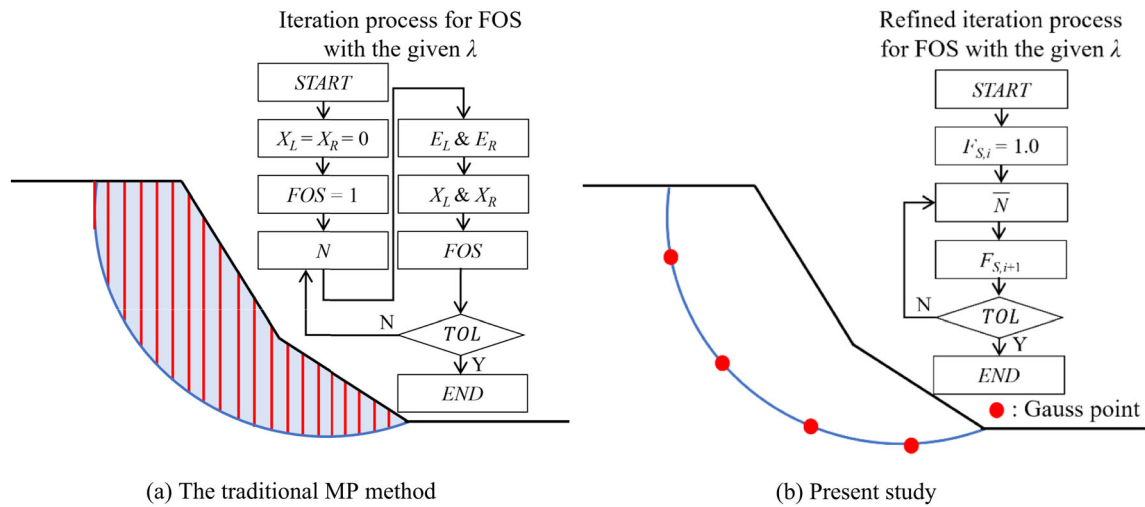


Fig. 1 Comparison between the traditional MP method and the present study

strength of the unsaturated soil named extended Mohr–Coulomb shear strength equation shown as follows has been introduced by Fredlund et al. [11], in which increasing rate of shear strength is related to matric suction:

$$\tau = c' + (\sigma - u_a) \tan \varphi' + (u_a - u_w) \tan \varphi^b \quad (1)$$

where  $\tau$  is the mobilized shear strength of the unsaturated soil;  $c'$  denote the effective cohesion intercept;  $\sigma$  is the normal stress;  $u_a$  and  $u_w$  represent the pore-air and the pore-water pressures, respectively;  $(\sigma - u_a)$  and  $(u_a - u_w)$  are the net normal stress at the failure plane and matric suction, respectively; and  $\varphi'$  and  $\varphi^b$  denote the effective angle of internal friction and the contribution of matric suction to the shear strength, respectively.

### 3.1 The traditional Morgenstern–Price method

#### 3.1.1 The factors of safety $F_m$ and $F_f$

Based on the shear strength of the unsaturated soil, the factor of safety under different equilibrium conditions can be calculated as follows [12]:

$$F_m = \frac{\sum_{i=1}^n \left\{ c'_i l_i R_i + \left[ N_i - u_{w,i} l_i \frac{\tan \varphi_i^b}{\tan \varphi_i'} - u_{a,i} l_i \left( 1 - \frac{\tan \varphi_i^b}{\tan \varphi_i'} \right) \right] R_i \tan \varphi_i' \right\}}{\sum_{i=1}^n W_i d_i - \sum_{i=1}^n N_i f_i} \quad (2)$$

$$F_f = \frac{\sum_{i=1}^n \left\{ c'_i l_i \cos \alpha_i + \left[ N_i - u_{w,i} l_i \frac{\tan \varphi_i^b}{\tan \varphi_i'} - u_{a,i} l_i \left( 1 - \frac{\tan \varphi_i^b}{\tan \varphi_i'} \right) \right] \cos \alpha_i \tan \varphi_i' \right\}}{\sum_{i=1}^n N_i \sin \alpha_i} \quad (3)$$

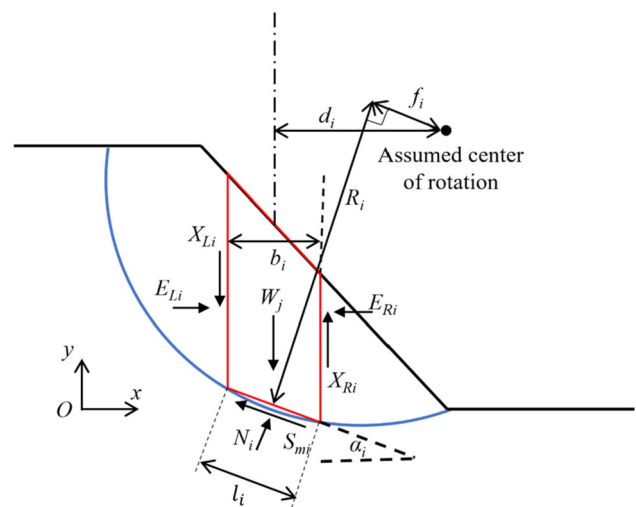


Fig. 2 Forces acting on one soil slice of a slope and slope geometry in the traditional MP method

where  $F_m$  and  $F_f$  are the FOSs when considering the moment equilibrium and lateral force conditions, respectively; the subscript  $i$  represents the indices of the soil slice;  $n$  is the slice number;  $l$  denotes the base length of the slice;  $N$  is the normal force at the slice base;  $W$  denotes the soil slice weight;  $R$  is the assumed radius;  $d$  represents the horizontal distance from the slice to the center of rotation;  $f$  is the perpendicular offset of the normal force from the center of rotation; and  $\alpha$  is the angle between the tangent to the center of the slice base and the horizontal. All the geometry parameters of the soil slices are plotted in Fig. 2. And the normal force,  $N$ , can be written as follows based on force equilibrium on vertical direction as well as mobilized shear force at slice base:

$$N_i = \frac{W_i - (X_{Ri} - X_{Li}) - \frac{c'_i l \sin \alpha_i}{F_s} + u_{a,i} \frac{l \sin \alpha_i}{F_s} (\tan \phi'_i - \tan \phi_i^b) + u_{w,i} \frac{l \sin \alpha_i}{F_s} \tan \phi_i^b}{m_{zi}} \quad (4)$$

$$X = \lambda f(x) E \quad (5)$$

$$E_{Ri} = E_{Li} + [W_i - (X_{Ri} - X_{Li})] \tan \alpha_i - \frac{S_{mi}}{\cos \alpha_i} \quad (6)$$

where

$$m_{zi} = \cos \alpha_i + \frac{\sin \alpha_i \tan \phi'_i}{F_s} \quad (7)$$

$$S_{mi} = \frac{1}{F_s} [c'_i l_i + N_i \tan \phi'_i + u_{a,i} l_i (\tan \phi_i^b - \tan \phi'_i) - u_{w,i} l_i \tan \phi_i^b] \quad (8)$$

in which,  $X$  and  $E$  denote the vertical and horizontal interslice forces, respectively; the subscripts  $L$  and  $R$  represent the left and right sides of the soil slice, respectively;  $F_s$  equals  $F_m$  when considering the moment equilibrium condition and equals  $F_f$  when considering the lateral force equilibrium condition;  $f(x)$  is a functional relationship which describes the magnitude of  $X/E$  varies across the slip surface;  $\lambda$  is the scaling factor for  $f(x)$ ; and  $S_m$  represents the mobilized shear force at the base of a slice.

### 3.1.2 Procedures for solving FOS

Different from the relatively simple algorithm in the Bishop method [3], the algorithms for calculating the FOSs in the MP method are relatively complicated. The analysis procedures of MP method mainly include two parts: (1) calculation of the values of  $F_m$  and  $F_f$  when the scaling factor  $\lambda$  is given; and (2) determination of the appropriate scaling factor  $\lambda$  that can satisfy  $F_m(\lambda) = F_f(\lambda)$  to fulfill both force and moment equilibrium conditions.

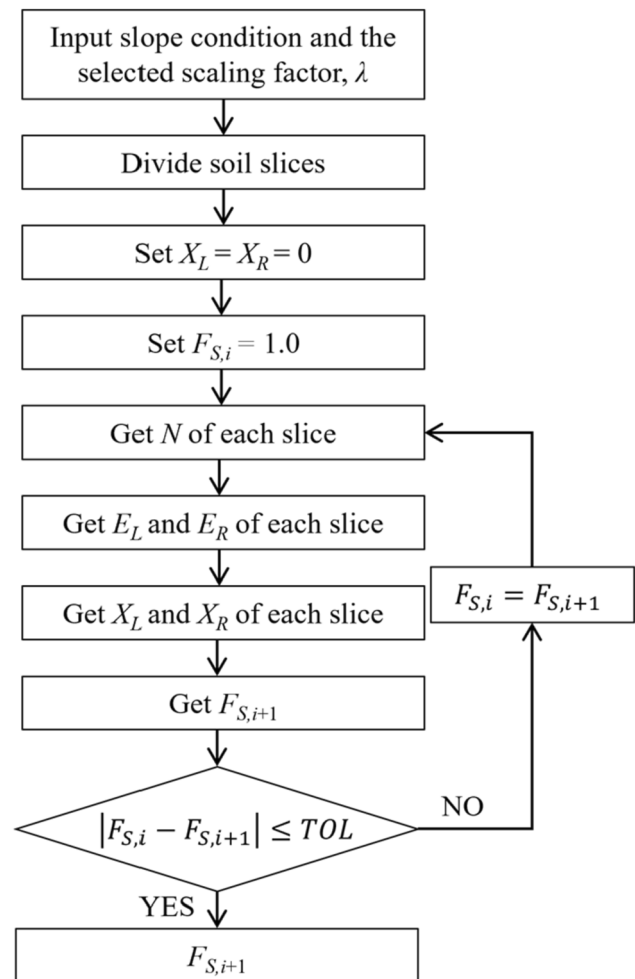


**Fig. 3** Solving FOS with the selected scaling factor in the traditional MP method

When obtaining the FOS values with the specific scaling factor  $\lambda$ , the calculation procedures (as demonstrated in Fig. 3) can be given as follows:

- (i) Input slope conditions and  $\lambda$ .
- (ii) Division of slices.
- (iii) Assume the interslice shear force  $X_L = X_R = 0$ .
- (iv) Set the FOS value equal to one,  $F_{s,i} = 1.0$ .
- (v) Get the slice normal force at each slice base,  $N$ , according to Eq. (4).
- (vi) Get the interslice shear force of each slice,  $E_L$ , and  $E_R$ , according to Eq. (6).
- (vii) Get the interslice normal force of each slice,  $X_L$  and  $X_R$ , according to Eq. (5).
- (viii) Calculate  $F_{s,i+1}$  according to Eq. (2) or Eq. (3).
- (ix) Set  $F_{s,i} = F_{s,i+1}$  and return to Step (iv) until the differences in values of  $F_s$  between two

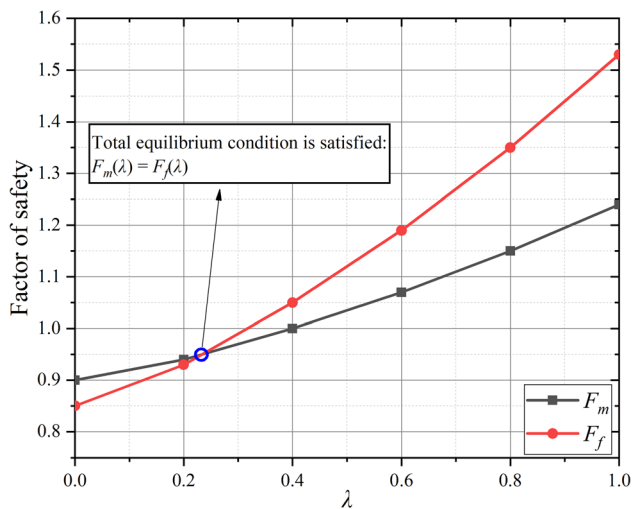


Fig. 4 Variation of FOS against scaling factor  $\lambda$

consecutive iterations are within specified limits of tolerance (*TOL*).

Different methods have been adopted for obtaining the appropriate scaling factor to satisfy  $F_m = F_f$ . Both Morgenstern and Price [23] and Zhu et al. [47] utilized the Newton–Raphson method to obtain the scaling factor during the analysis. Cheng [5] introduced the double QR

factorization method as the solution technique for determining the FOS. However, both the Newton–Raphson method and the double QR factorization method require complicated gradient formulas or solving process during calculations, posing significant challenges for implementation. Fredlund and Krahn [10] presented an alternate procedure for searching the scaling factor based on the best-fit regression method, which is easier to be implemented. The best-fit method selects several reasonable scaling factors to obtain the corresponding FOS values when considering the moment and force equilibrium conditions. Then, total equilibrium condition is satisfied at a point when curves of  $F_m$  and  $F_f$  intersect at a point (as shown in Fig. 4).

### 3.2 The improved Morgenstern–Price method

#### 3.2.1 The factors of safety $F_m$ and $F_f$

In LEM, the slice division must be dense enough by increasing the slice number to achieve the reliable results. When the slice of width,  $b_i$ , trends to be infinitesimally small and the slice number,  $n$ , is infinite, Eqs. (2) and (3) can be rewritten as follows:

$$\begin{aligned}
 F_m &= \lim_{b_i \rightarrow 0} \frac{\sum_{i=1}^{\infty} \left\{ c'_i l_i R_i + \left[ N_i - u_{w,i} l_i \frac{\tan \varphi_i^b}{\tan \varphi_i'} - u_{a,i} l_i \left( 1 - \frac{\tan \varphi_i^b}{\tan \varphi_i'} \right) \right] R_i \tan \varphi_i' \right\}}{\sum_{i=1}^{\infty} W_i d_i - \sum_{i=1}^{\infty} N_i f_i} \\
 &= \lim_{b_i \rightarrow 0} \frac{\sum_{i=1}^{\infty} \left\{ c'_i \frac{b_i}{\cos \alpha_i} R_i + \left[ N_i - u_{w,i} \frac{b_i}{\cos \alpha_i} \frac{\tan \varphi_i^b}{\tan \varphi_i'} - u_{a,i} \frac{b_i}{\cos \alpha_i} \left( 1 - \frac{\tan \varphi_i^b}{\tan \varphi_i'} \right) \right] R_i \tan \varphi_i' \right\}}{\sum_{i=1}^{\infty} b_i \rho_i d_i - \sum_{i=1}^{\infty} \frac{N_i}{b_i} b_i f_i} \tag{9} \\
 &= \frac{\int \left\{ c' \frac{R}{\cos \alpha} + \left[ \frac{dN}{dx} - \frac{u_w}{\cos \alpha} \frac{\tan \varphi^b}{\tan \varphi'} - \frac{u_a}{\cos \alpha} \left( 1 - \frac{\tan \varphi^b}{\tan \varphi'} \right) \right] R \tan \varphi' \right\} dx}{\int (\rho d) dx - \int \left( \frac{dN}{dx} f \right) dx}
 \end{aligned}$$

$$\begin{aligned}
 F_f &= \lim_{b_i \rightarrow 0} \frac{\sum_{i=1}^{\infty} \left\{ c'_i l_i \cos \alpha_i + \left[ N_i - u_{w,i} l_i \frac{\tan \varphi_i^b}{\tan \varphi_i'} - u_{a,i} l_i \left( 1 - \frac{\tan \varphi_i^b}{\tan \varphi_i'} \right) \right] \cos \alpha_i \tan \varphi_i' \right\}}{\sum_{i=1}^{\infty} N_i \sin \alpha_i} \\
 &= \lim_{b_i \rightarrow 0} \frac{\sum_{i=1}^{\infty} \left\{ c'_i \frac{b_i}{\cos \alpha_i} \cos \alpha_i + \left[ N_i \cos \alpha_i - u_{w,i} b_i \frac{\tan \varphi_i^b}{\tan \varphi_i'} - u_{a,i} b_i \left( 1 - \frac{\tan \varphi_i^b}{\tan \varphi_i'} \right) \right] \tan \varphi_i' \right\}}{\sum_{i=1}^{\infty} N_i \sin \alpha_i} \tag{10} \\
 &= \frac{\int \left\{ c' + \left[ \frac{dN}{dx} \cos \alpha - u_w \frac{\tan \varphi^b}{\tan \varphi'} - u_a \left( 1 - \frac{\tan \varphi^b}{\tan \varphi'} \right) \right] \tan \varphi' \right\} dx}{\int \left( \frac{dN}{dx} \sin \alpha \right) dx}
 \end{aligned}$$

where  $dx$  denotes width of an infinitesimal soil slice;  $\rho$  is the weight of the slice per unit width; and  $dN/dx$  is normal force at the base of the slice per unit width.

According to Eqs. (4) to (8), the interslice force and the normal force acting on the infinitesimally thin slice can be expressed as:

$$dN = \frac{\rho dx - dX - \frac{c'}{F_s} \tan \alpha dx + u_a \frac{\tan \alpha}{F_s} (\tan \phi' - \tan \phi^b) dx + u_w \frac{\tan \phi^b}{F_s} \tan \alpha dx}{m_x} \quad (11)$$

$$dX = \lambda f(x) dE \quad (12)$$

$$dE = (\rho \tan \alpha) dx - \tan \alpha dX - \frac{1}{\cos \alpha} dS_m \quad (13)$$

where,

$$dS_m = \frac{1}{F_s} \left\{ \frac{c'}{\cos \alpha} dx + \tan \phi' dN + \left[ \frac{u_a}{\cos \alpha} (\tan \phi^b - \tan \phi') - \frac{u_w}{\cos \alpha} \tan \phi^b \right] dx \right\} \quad (14)$$

Only four unknown variables, including  $dN$ ,  $dX$ ,  $dE$ , and  $dS_m$ , within the above linear equation group, are observed. Thus, by rearranging Eqs. (11) to (14),  $dN$  can be obtained as:

$$dN = \frac{1}{\bar{m}_x} \left[ \rho - \frac{c'}{F_s} \tan \alpha + u_a \frac{\tan \alpha}{F_s} (\tan \phi' - \tan \phi^b) + u_w \frac{\tan \alpha}{F_s} \tan \phi^b \right] dx + \frac{1}{\bar{m}_x \lambda f(x) F_s} [c' + u_a (\tan \phi^b - \tan \phi') - u_w \tan \phi^b] dx \quad (15)$$

where,

$$\bar{m}_x = m_x + \lambda f(x) \left( \sin \alpha - \cos \alpha \frac{\tan \phi'}{F_s} \right) \quad (16)$$

But even the expression of  $dN$  is obtained, the analytical solutions for Eqs. (9) and (10) are still hard to be derived. Thus, a numerical integral technique, named the Gaussian integral, is introduced for simplifying the expression of FOSs. Using the Gaussian integral, Eqs. (9) and (10) can be rewritten as:

$$F_m = \frac{\sum_{j=1}^{NG} \omega_j \left\{ c'_j \frac{R_{kj}}{\cos \alpha_j} + \left[ \bar{N}_j - \frac{u_{w,j} \tan \phi_j^b}{\cos \alpha_j \tan \phi_j'} - \frac{1}{\cos \alpha_j} u_{a,j} \left( 1 - \frac{\tan \phi_j^b}{\tan \phi_j'} \right) \right] R_j \tan \phi_j' \right\}}{\sum_{j=1}^{NG} \omega_j (\rho_j d_j) - \sum_{j=1}^{NG} \omega_j (\bar{N}_j f_j)} \quad (17)$$

$$F_f = \frac{\sum_{j=1}^{NG} \omega_j \left\{ c'_j + \left[ \bar{N}_j \cos \alpha_j - u_{w,j} \frac{\tan \phi_j^b}{\tan \phi_j'} - u_{a,j} \left( 1 - \frac{\tan \phi_j^b}{\tan \phi_j'} \right) \right] \tan \phi_j' \right\}}{\sum_{j=1}^{NG} \omega_j (\bar{N}_j \sin \alpha_j)} \quad (18)$$

where,

$$\bar{N} = \frac{1}{\bar{m}_x} \left[ \rho - \frac{c'}{F_s} \tan \alpha + u_a \frac{\tan \alpha}{F_s} (\tan \phi' - \tan \phi^b) + u_w \frac{\tan \alpha}{F_s} \tan \phi^b \right] + \frac{1}{\bar{m}_x \lambda f(x) F_s} [c' + u_a (\tan \phi^b - \tan \phi') - u_w \tan \phi^b] \quad (19)$$

in which,  $NG$  is the number of Gauss points; the subscript  $j$  denotes the number of Gauss point; and  $\omega$  is the weight coefficient of Gauss point.

To maintain the function's continuity within the domain, the slip surface should be divided into several integration intervals when the present study is employed for some slip surfaces with gradient-discontinuity points or passing through interfaces of soil layers. Therefore, the FOS expressions can be further rewritten for generality as:

$$F_m = \frac{\sum_{k=1}^{NI} (x^k - x^{k-1}) \sum_{j=1}^{NG} \omega_{kj} \left\{ c'_{kj} \frac{R_{kj}}{\cos \alpha_{kj}} + \left[ \bar{N}_{kj} - \frac{u_{w,kj} \tan \phi_{kj}^b}{\cos \alpha_{kj} \tan \phi_{kj}'} - \frac{1}{\cos \alpha_{kj}} u_{a,kj} \left( 1 - \frac{\tan \phi_{kj}^b}{\tan \phi_{kj}'} \right) \right] R_{kj} \tan \phi_{kj}' \right\}}{\sum_{k=1}^{NI} (x^k - x^{k-1}) \sum_{j=1}^{NG} \omega_{kj} (\rho_{kj} d_{kj}) - \sum_{k=1}^{NI} (x^k - x^{k-1}) \sum_{j=1}^{NG} \omega_{kj} (\bar{N}_{kj} f_{kj})} \quad (20)$$

$$F_f = \frac{\sum_{k=1}^{NI} (x^k - x^{k-1}) \sum_{j=1}^{NG} \omega_{kj} \left\{ c'_{kj} + \left[ \bar{N}_{kj} \cos \alpha_{kj} - u_{w,kj} \frac{\tan \phi_{kj}^b}{\tan \phi_{kj}'} - u_{a,kj} \left( 1 - \frac{\tan \phi_{kj}^b}{\tan \phi_{kj}'} \right) \right] \tan \phi_{kj}' \right\}}{\sum_{k=1}^{NI} (x^k - x^{k-1}) \sum_{j=1}^{NG} \omega_{kj} (\bar{N}_{kj} \sin \alpha_{kj})} \quad (21)$$

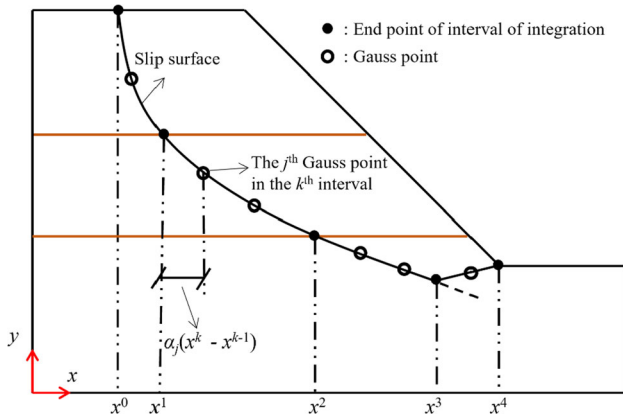


Fig. 5 Alignment of Gauss points in the proposed method

where  $NI$  denotes the number of intervals of integration; the subscript  $k$  is the number of the interval of integration; and  $x^{k-1}$  and  $x^k$  are two end points of the interval of integration, which should be the intersection point between the slip surface or the gradient-discontinuity point of the slip surface (as demonstrated in Fig. 5).

The location of the adopted Gauss point,  $(x_{kj}, y_{kj})$ , can be calculated as follows:

$$x_{kj} = \alpha_j(x^k - x^{k-1}) + x^{k-1} \quad (22)$$

$$y_{kj} = S(x_{kj}) \quad (23)$$

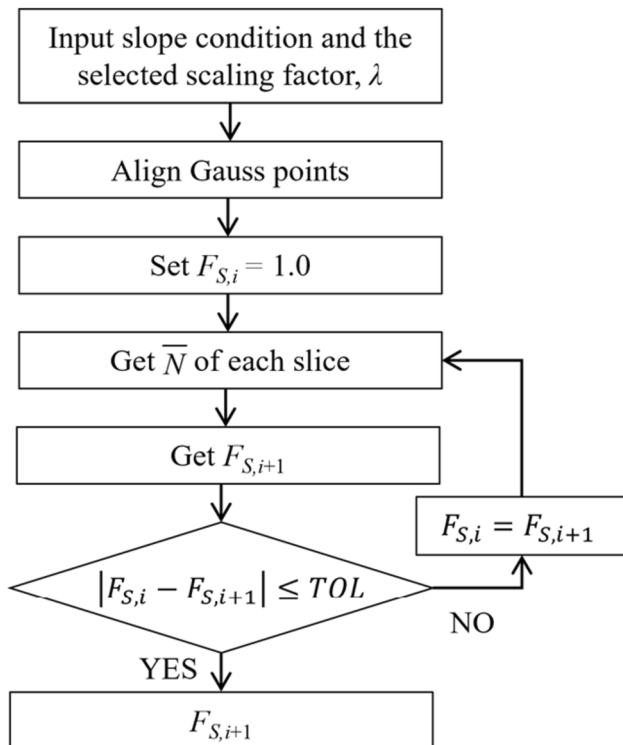


Fig. 6 Solving FOS with the selected scaling factor in the present study

where  $\alpha$  is the dimensionless coefficient of Gauss point; and  $S(x)$  is the shape function of the slip surface. It is recommended to use 3–5 Gauss points in one integral region to achieve reliable results. More Gauss points can also be defined based on the specific situation.

### 3.2.2 Refined procedures for solving FOS

The solving procedures for the FOS in the present study include two parts: (1) solving the FOS with the selected scaling factor; (2) obtaining the scaling factor satisfying the total equilibrium conditions.

When solving factor of safety equations in the traditional MP method, the interslice force distribution must be assumed to be zero initially. Then, in each iterative step, the interslice force should be updated separately, leading to a tedious computational procedure. In the present study, a set of more concise iteration procedures (see Fig. 6) can be described as follows:

- (i) Input slope conditions and  $\lambda$ .
- (ii) Align Gauss points.
- (iii) Set  $F_{s,i} = 1.0$ .
- (iv) Get the normal force at each Gauss point,  $\bar{N}$ , according to Eq. (19).
- (v) Calculate  $F_{s,i+1}$  according to Eq. (20) or Eq. (21).
- (vi) Set  $F_{s,i} = F_{s,i+1}$  and return to Step (iv) until the differences in values of  $F_s$  between two consecutive iterations are within specified limits of tolerance,  $TOL$ .

It is convenient to implement the best-fit regression method for searching the scaling factor for the total equilibrium condition. However, the data points must be

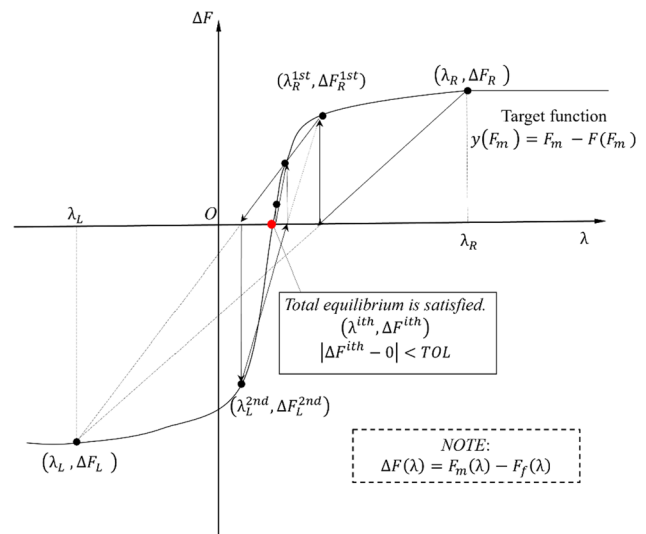
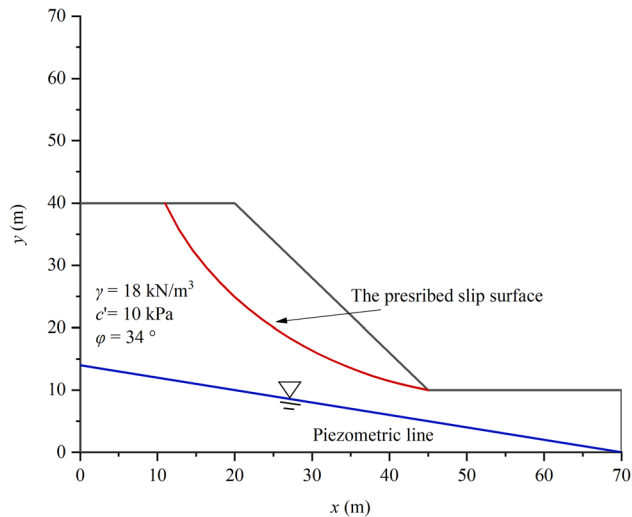


Fig. 7 Schematic diagram of linear search algorithm for determining the scaling factor



**Fig. 8** Geometry and prescribed critical slip surface of a homogenous unsaturated soil slope

**Table 1** FOS under different values of  $\phi^b$  for the example of a homogenous unsaturated soil slope

$\phi^b$ (°)	FOS in Zhang et al. [44]	FOS in present study	Error (%)
0	1.005	1.001	0.39
15°	1.430	1.426	0.28
34°	2.118	2.121	0.14

distributed densely enough to searching the accurate results of the joining between  $F_m$  and  $F_f$  (as shown in Fig. 4), implying that the relatively large computational effort is taken in the analysis. For efficiently searching the scaling factor satisfying both moment and force equilibrium conditions, a linear searching method is employed in the present study. The linear searching method (as illustrated in Fig. 7) can be described as follows:

- (i) Input the searching range  $[\lambda_L, \lambda_R]$ .
- (ii) Obtain  $\Delta F(\lambda_L)$  and  $\Delta F(\lambda_R)$ , where  $\Delta F(\lambda) = F_m(\lambda) - F_f(\lambda)$ .
- (iii) Calculate  $\lambda_M$  using the secant relation as:
 
$$\lambda_M = \frac{\lambda_L \Delta F(\lambda_R) + \lambda_R \Delta F(\lambda_L)}{\Delta F(\lambda_R) - \Delta F(\lambda_L)}$$
- (iv) Check whether  $\Delta F(\lambda_M)$  achieves the convergence criterion. If the convergence tolerance is satisfied, output  $\lambda_M$  as the result. Otherwise, return to Step (iv) and update the searching range according to:

$$\lambda_L = \begin{cases} \lambda_L & \text{if } \Delta F(\lambda_L)\Delta F(\lambda_M) < 0 \\ \lambda_M & \text{if } \Delta F(\lambda_L)\Delta F(\lambda_M) \geq 0 \end{cases} \quad \text{AND} \quad \lambda_R = \begin{cases} \lambda_R & \text{if } \Delta F(\lambda_R)\Delta F(\lambda_M) < 0 \\ \lambda_M & \text{if } \Delta F(\lambda_R)\Delta F(\lambda_M) \geq 0 \end{cases}$$

**Table 2** FOS and computational cost in different methods for the example of a homogenous slope

Analysis method	$n_{SP}$	$\phi^b$ (°)	FOS	Computational time (s)
Traditional MP	32 slices	0	0.887	1202
		15	1.420	1532
		34	1.908	1598
Present study	5 Gauss points	0	0.895	113
		15	1.399	122
		34	1.879	185

Notes:  $n_{SP}$  denotes the number of sampling points in different methods

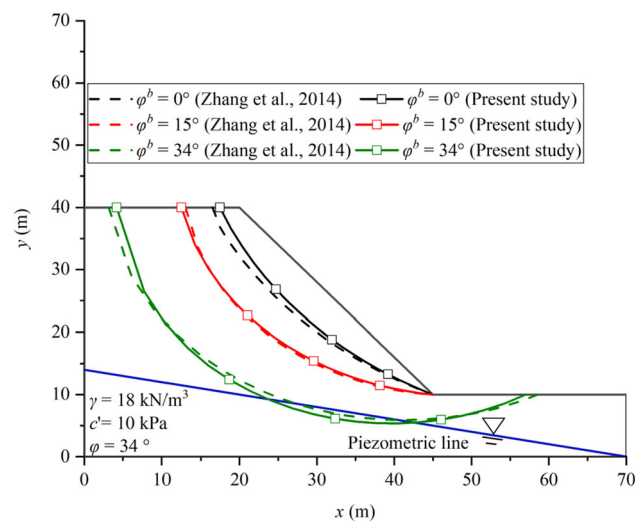


**Fig. 9** Critical slip surfaces based on present study and traditional MP method for a homogenous unsaturated soil slope

## 4 Computer program

A computer program, named PyGEOSlope, has been developed in the Hong Kong Polytechnic University to evaluate the stability of unsaturated soil slopes [25]. Both traditional and improved MP methods can be adopted in this program. The program for unsaturated soil slopes based on Gaussian integral is validated by several examples and case studies in this study. This program can also



be used to explore its potential use in the further studies for different practical stability problems for saturated and unsaturated soil slopes. Due to the potential problems in evaluating stability of unsaturated soil slopes, such as complex soil behavior and low efficiency, the authors hope to promote more innovative and efficient methods to obtain reliable evaluation for stability of saturated and unsaturated soil slopes.

### 5 Verification examples

In this section, two typical types of slopes are studied to validate the present method based on Gaussian integral for assessing the stability of unsaturated soil slopes, including homogeneous and nonhomogeneous slopes.

#### 5.1 Example 1: Stability analysis of a homogeneous unsaturated soil slope

In this example, a steep and homogeneous slope with a height of 30 m and a slope angle of 50° is re-analyzed [44]. Figure 8 illustrates the geometry of this homogenous steep slope and prescribed critical slip surface. The unit weight of the soil is  $\gamma = 18 \text{ kN/m}^3$ . The cohesion and effective internal friction angle of the soil are  $c' = 10 \text{ kPa}$  and  $\phi' = 34^\circ$ , respectively. The average depth of piezometric line is more than 10 m below the surface of slope.

A specific slip surface is selected for evaluating the stability of this unsaturated soil slope (see Fig. 8). Table 1 lists the values of FOS of the slope with the prescribed slip surface under different  $\phi^b$  values. The FOS values of the unsaturated soil slope in this study are generally consistent with those calculated by Zhang et al. [44]. The FOS of

slope increases gradually with the increase of  $\phi^b$ . This increasing trend is because the increasing  $\phi^b$  has enhanced the shear strength listed in Eq. (1), and thus, the enhancing mobilized shear force shown in Eq. (8) at the slice base increases. The error is also evaluated, which is defined by ratio of difference between the previous value of FOS and FOS in the present study to the FOS in the present study. The error decreases with the increase of  $\phi^b$ .

The traditional MP method has also been used to validate the new method in present study. The numbers of soil slices for traditional MP method and Gauss points for present study are 32 and 5, respectively. Table 2 summarizes the FOS and computational cost in the present proposed and traditional MP methods for this example. The improved MP method using Gaussian integral with only five Gauss points shows much higher efficiency than the traditional MP method with 32 slices, no matter which value of  $\phi^b$  is assumed. In general, for different values of  $\phi^b$ , the time used in the present study is approximately only one-tenth of that used in the traditional MP method. Figure 9 shows comparisons of critical slip surfaces based on the present study and traditional MP method for the homogenous slope. The critical slip surfaces obtained from the present study agree well with those surfaces suggested by Zhang et al. [44]. The depth of critical slip surface increases with the rising  $\phi^b$ . Compared with the other two critical slip surfaces, the critical slip surface for  $\phi^b = \phi'$  is much deeper. This example demonstrates the accuracy and efficiency of this improved MP method in evaluating the stability of unsaturated and homogenous soil slope. In addition, Table 2 also demonstrates that ignoring unsaturated characteristic of soil by taking  $\phi^b = 0^\circ$  will lead to significant underestimation of slope stability, underscoring

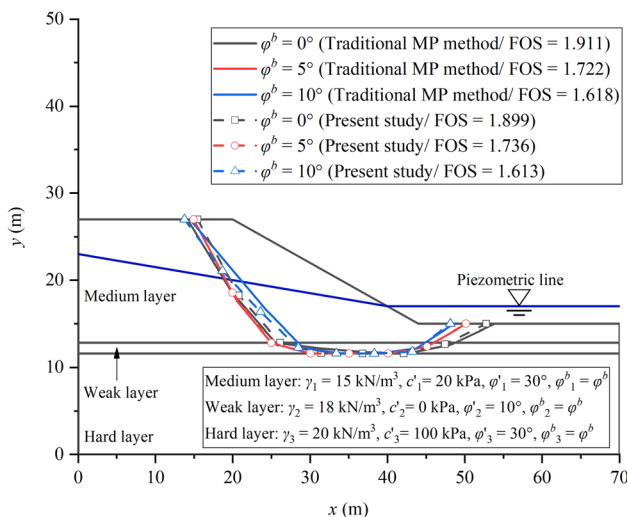


Fig. 10 Critical slip surfaces based on present study and traditional MP method for a nonhomogeneous unsaturated soil slope

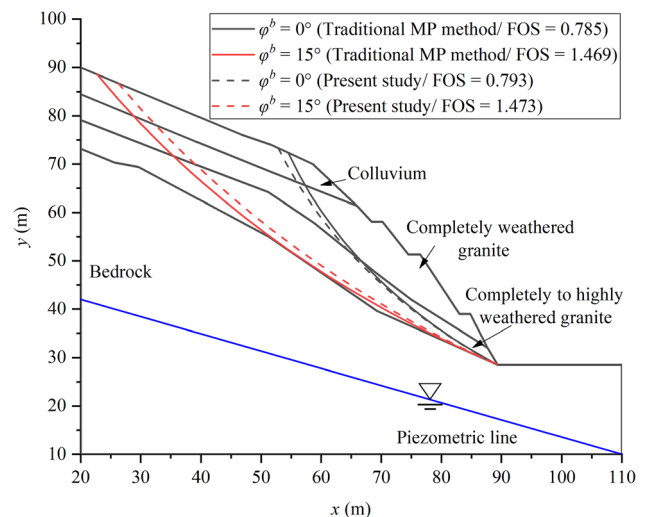


Fig. 11 Critical slip surfaces based on present study and traditional MP method for an unsaturated soil slope of weathered granite

the critical need to accurately account for the unsaturated properties of soil in slope stability assessment.

## 5.2 Example 2: Stability analysis of a nonhomogeneous unsaturated soil slope

Example 2 was originally presented by Fredlund et al. [12]. The example is a nonhomogeneous slope with three layers, in which there is a weak layer between medium and hard layers. The geometry, soil properties of different layers, and piezometric line are shown in Fig. 10. Fredlund et al. [12] compared the values of FOS based on dynamic programming method and MP method and found that FOS of dynamic programming method was around 14% lower than that of MP method. The critical slip surface is highly irregular and influenced by the position of weak layer.

Here, the example is re-analyzed using the proposed method and traditional MP method. In this example, three–four Gauss points are aligned at each soil layer in the proposed method. The different values of FOS for different values of  $\varphi^b$  based on these two methods are shown in Fig. 10. In general, with the rise of  $\varphi^b$ , the critical slip surface gets shallower for the two methods. The shape of critical slip surfaces changes from a typical circular arc to an irregular shape. It seems that the position of weak layer affects the shape of critical slip surfaces and leads to the irregular shape of critical slip surfaces. This phenomenon agrees well with those observed by Fredlund et al. [12]. For both two methods, the FOS decreases with the increase of  $\varphi^b$ . The declining trend of FOS with increasing  $\varphi^b$  for the nonhomogeneous slope is different from the increasing trend observed in a homogeneous slope since the FOS is influenced by the combination of factors, such as soil layers, soil properties, and piezometric line. The FOS results based on proposed method are generally consistent with those based on the traditional MP method. This

**Table 3** Soil properties in case study 1 and case study 2

Case study no	Soil type	$\gamma$ (kN/m <sup>3</sup> )	$c'$ (kPa)	$\varphi'$ (°)	$\varphi^b$ (°)
Case study 1	Colluvium	19.6	10.0	35.0	15.0
	Completely weathered granite	19.6	15.1	35.2	15.0
	Completely to highly weathered granite	19.6	23.5	41.5	15.0
Case study 2	Completely weathered rhyolite	18.4	10.1	42.6	12.0
	Completely to highly weathered rhyolite	21.4	12.0	43.9	12.0

example shows the effectiveness and accuracy of this proposed method in evaluation of stability of nonhomogeneous slope.

## 6 Case studies

Two case studies of typical residual soil slopes in Hong Kong are re-analyzed in this section to validate the present proposed method for evaluating the stability of unsaturated soil slopes [12]. In these two cases, boreholes were drilled to obtain the soil stratigraphy and intact soil samples. The suction-controlled triaxial tests were conducted on these intact soil samples to determine the shear strength parameters of soils, such as  $c'$ ,  $\varphi'$  and  $\varphi^b$ . In the field, soil suctions (negative pore-water pressures) were measured by tensiometers.

### 6.1 Case study 1: Stability analysis of a cut slope of weathered granite

As shown in Fig. 11, case study 1 is a steep cut slope of weathered granite behind a hospital and residential buildings in Hong Kong. There have been dangerous small periodic failures at the crest of slope, which require a comprehensive investigation. The average inclination of the slope is 60°. The slope surface is a layer of soil cement and lime plaster which can protect the slope from water infiltration. The soil stratigraphy is broadly distributed in Hong Kong especially for the colluvial slopes in the mountain area, including granitic colluvium, completely weathered granite, and highly weathered granite. The weathered granite is one of the most common residual soils in Hong Kong. The depth of bedrock is 20 to 30 m below

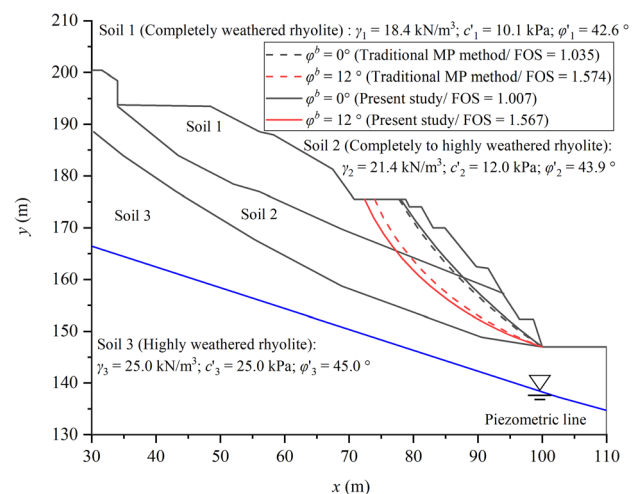


**Fig. 12** Critical slip surfaces based on present study and traditional MP method for an unsaturated soil slope of weathered rhyolite

**Table 4** Computational cost of different methods in case study 2

Analysis method	$\varphi^b$ (°)	Computational time (s)
Traditional MP using 50 slices	0	1206
	12	3586
Present study	0	231
	12	235

the ground surface. The approximate position of water table is located in the bedrock. Table 3 lists the soil properties of different layers in case study 1. The average value of  $\varphi^b$  is 15.0° based on the results of triaxial tests [14]. The measured soil suction ranges from approximately 0 to 80 kPa due to different elevations. With the increase in elevation, the soil suction gets greater.

This case study has been re-analyzed by comparing the slope stability evaluation using the efficient LEM based on Gaussian integral and the traditional MP method (see Fig. 10). Three–four Gauss points are placed in each soil layer in this case study. In the analysis, the suction was ignored ( $\varphi^b = 0^\circ$ ) firstly. The FOS values based on the traditional MP method and present method are 0.785 and 0.793, respectively. These results can generally agree well with the FOS of 0.864 based on the Bishop simplified method [12]. These slight differences might be due to the different assumptions in these methods, such as different force equilibrium conditions and soil discretization methods. Nevertheless, it seems that the slope is still stable. This might be attributed to the enhanced shearing strength because suction has strengthened the slope stability, reflecting the significant role of suction in soil slope stability. Secondly, the average value of  $\varphi^b$ , which is equal to 15.0°, was adopted in the analysis. The values of FOS for the traditional MP method and present method are 1.469 and 1.473, respectively. It shows that the consideration of suction has greatly enhanced the slope stability. In addition, the critical slip surfaces based on these two methods are consistent with each other no matter whether the suction is considered or not. With the increase of  $\varphi^b$ , the depth of critical slip surface gets deeper. These results of FOS values and critical slip surfaces agree well with those observed by Zhang et al. [44].

## 6.2 Case study 2: Stability analysis of a cut slope of weathered rhyolite

In case study 2, a high and steep cut slope of weathered rhyolite located behind a residential building is re-analyzed (see Fig. 12). The inclination of the slope is 60°. The soil stratigraphy consists of completely and highly weathered

rhyolite, which is another typical common weathered soil in Hong Kong. The approximate water table is in highly weathered rhyolite below the ground surface. The matric suction was measured by tensiometers through a rainy season. In general, the profiles of matric suction kept stable except some variations at the ground surface due to the water infiltration with fluctuations of water table.

The stability of the high and steep cut slope was re-assessed using the traditional MP method and efficient LEM based on Gaussian integral. There are three–four Gauss points aligned in each soil layer in this case study. Table 3 lists the soil properties of the soil layers in case study 2. As shown in Fig. 12, different suction effects on shearing strength ( $\varphi^b = 0^\circ$  and 12°) were assumed in the analysis. For both two methods, FOS increases with the increase of  $\varphi^b$ . Table 4 lists the computational cost of different methods in case study 2. The proposed method has greatly improved the computational efficiency. Despite the analyses being conducted on an identical computing device, equipped with 16 GB RAM and an Intel Core i7 CPU, the computational time required by the current method is notably reduced to approximately 1/5 to 1/10 of that necessitated by the traditional MP method. The values of FOS for these two methods agree well with each other. The critical slip surfaces based on these two methods can accord with each other for different values of  $\varphi^b$ . The shapes of the critical slip surfaces are circular arcs, and the depth of critical slip surface gets deeper with rising  $\varphi^b$ . All of the critical slip surfaces go across the slope toe. Overall, it can be concluded that the new efficient LEM based on Gaussian integral is reliable, accurate, and efficient.

## 7 Conclusions

This study presents an efficient numerical implementation of limit equilibrium method (LEM) based on the Morgenstern–Price method using Gaussian integral for stability analysis of unsaturated soil slopes. This new method is an extension of the improved Morgenstern–Price method proposed by Ouyang et al. [26]. Compared with the other methods, this method may be a useful attempt and might provide a new solution to evaluate the stability of unsaturated soil slopes. Conclusions are mainly summarized as follows:

- (1) The extended Mohr–Coulomb shear strength equation is adopted to be the governing shearing strength equation in the analysis of slope stability [11]. In traditional LEM, the slice division shall be dense enough by increasing the slice number to achieve reliable results. However, in the new method, a numerical integral technique, named Gaussian

integral, is introduced for simplifying the expressions and calculations of FOS values. In addition, the solving procedures for the FOS in the present study mainly include two parts, including solving the FOS with the selected scaling factor and determining the scaling factor satisfying the total equilibrium conditions. Based on the developed formula, the iteration process for calculating the FOS with the given scaling factor is refined where the step of assuming the initial force distribution is eliminated. Besides, the linear search method is used in searching the scaling factor to fulfill the total equilibrium conditions. Finally, these FOS formulas have been incorporated into a new computer program, named PyGEOSlope, to systematically evaluate the stability of saturated and unsaturated soil slopes.

- (2) This new method is validated based on two typical benchmark examples such as homogeneous and nonhomogeneous unsaturated soil slopes and two case studies of unsaturated residual soil slopes in Hong Kong. Overall, compared with the traditional MP method, the newly proposed method with a few Gauss points is reliable, accurate, and efficient in evaluating the stability of unsaturated soil slopes.

In the future, for engineering applications, this study may be extended for slopes with special types of soils such as gap-graded soil [29, 32], mixed soils [30, 35, 36, 41], layered soil [18], etc.

**Acknowledgements** The Start-up Fund for RAPs under the Strategic Hiring Scheme from PolyU (UGC) (Project ID: P0045938) is acknowledged. The authors also acknowledge the supports by a RIF project (Grant No.: R5037-18) and GRF projects (Grant No.: 15217918, 15213019, 15210020, 15231122) from Research Grants Council (RGC) of Hong Kong Special Administrative Region Government of China. The authors also acknowledge the financial support from grants (CD7A and CD82) from the Research Institute for Land and Space of Hong Kong Polytechnic University, and financial support (W23L, ZDBS) from The Hong Kong Polytechnic University. This financial support is gratefully acknowledged. This work is also partially supported by grants from the Research Grants Council of the Hong Kong Special Administrative Region, China (Grant No.: 15203121).

**Funding** Open access funding provided by The Hong Kong Polytechnic University.

**Data availability** Some or all data, models, or code that supports the findings of this study is available from the corresponding author upon reasonable request.

## Declarations

**Conflict of interest** The authors declare that they have no know competing financial interests or personal relationships that could have appeared to influence the work reported in this paper.

**Open Access** This article is licensed under a Creative Commons Attribution 4.0 International License, which permits use, sharing, adaptation, distribution and reproduction in any medium or format, as long as you give appropriate credit to the original author(s) and the source, provide a link to the Creative Commons licence, and indicate if changes were made. The images or other third party material in this article are included in the article's Creative Commons licence, unless indicated otherwise in a credit line to the material. If material is not included in the article's Creative Commons licence and your intended use is not permitted by statutory regulation or exceeds the permitted use, you will need to obtain permission directly from the copyright holder. To view a copy of this licence, visit <http://creativecommons.org/licenses/by/4.0/>.

## References

- Bai T, Qiu T, Huang X, Li C (2014) Locating global critical slip surface using the Morgenstern-Price method and optimization technique. *Int J Geomech* 14(2):319–325
- Biniyaz A, Azmoon B, Liu Z (2022) Coupled transient saturated–unsaturated seepage and limit equilibrium analysis for slopes: influence of rapid water level changes. *Acta Geotech* 17(6):2139–2156
- Bishop AW (1955) The use of the slip circle in the stability analysis of slopes. *Géotechnique* 5(1):7–17
- Cai F, Ugai K (2004) Numerical analysis of rainfall effects on slope stability. *Int J Geomech* 4(2):69–78
- Cheng YM (2003) Location of critical failure surface and some further studies on slope stability analysis. *Comput Geotech* 30(3):255–267
- Cheng YM, Lau C (2014) *Slope stability analysis and stabilization: new methods and insight*. CRC Press, Boca Raton
- Cho SE, Lee SR (2001) Instability of unsaturated soil slopes due to infiltration. *Comput Geotech* 28(3):185–208
- Duncan MJ (1996) State of the art: limit equilibrium and finite-element analysis of slopes. *J Geotech Eng* 122(7):577–596
- Fathipour H, Tajani SB, Payan M et al (2023) Impact of transient infiltration on the ultimate bearing capacity of obliquely and eccentrically loaded strip footings on partially saturated soils. *Int J Geomech* 23(2):1–19
- Fredlund DG, Krahn J (1977) Comparison of slope stability methods of analysis. *Can Geotech J* 14(3):429–439
- Fredlund DG, Morgenstern NR, Widger RA (1978) The shear strength of unsaturated soils. *Can Geotech J* 15(3):313–321
- Fredlund DG, Rahardjo H, Fredlund MD (2012) *Unsaturated soil mechanics in engineering practice*. Wiley, New York
- Griffiths DV, Lu N (2005) Unsaturated slope stability analysis with steady infiltration or evaporation using elasto-plastic finite elements. *Int J Numer Anal Methods Geomech* 29(3):249–267
- Ho DYF, Fredlund DG (1982) Increase in strength due to suction for two Hong Kong soils. In: *Proceedings of the ASCE specialty conference on engineering and construction in tropical and residual soils, Hawaii*, pp 263–295
- Houston SL (2019) It is time to use unsaturated soil mechanics in routine geotechnical engineering practice. *J Geotech Geoenviron Eng* 145(5):02519001
- Huang W, Ji J (2023) Upper bound seismic limit analysis of shallow landslides with a new kinematically admissible failure mechanism. *Acta Geotech* 18(5):2473–2485
- Janbu N (1973) *Slope stability computations*. Wiley, New York.
- Li C, Wu J, Tang H, Hu X, Liu X, Wang C, Liu T, Zhang Y (2016) Model testing of the response of stabilizing piles in landslides with upper hard and lower weak bedrock. *Eng Geol* 204:65–76

19. Liu K, Yin JH, Chen WB et al (2020) The stress–strain behaviour and critical state parameters of an unsaturated granular fill material under different suctions. *Acta Geotech* 15(12):3383–3398
20. Liu K, Yin ZY, Chen WB et al (2021) Nonlinear model for the stress–strain–strength behavior of unsaturated granular materials. *Int J Geomech* 21(7):04021103
21. Liu X, Li DQ, Cao ZJ, Wang Y (2020) Adaptive Monte Carlo simulation method for system reliability analysis of slope stability based on limit equilibrium methods. *Eng Geol* 264(October 2019):105384
22. Meng J, Li C, Zhou JQ, Zhang Z, Yan S, Zhang Y, Huang D, Wang G (2023) Multiscale evolution mechanism of sandstone under wet-dry cycles of deionized water: from molecular scale to macroscopic scale. *J Rock Mech Geotech Eng* 15(5):1171–1185
23. Morgenstern NR, Price VE (1965) The analysis of the stability of general slip surfaces. *Géotechnique* 15(1):79–93
24. Ng CWW, Shi Q (1998) A numerical investigation of the stability of unsaturated soil slopes subjected to transient seepage. *Comput Geotech* 22(1):1–28
25. Ouyang WH, Liu K, Liu SW, Yin JH (2022) Improved morgenstern-price slope analysis program in Python—PyGEOSlope for unsaturated soil slopes (Version 1.0), Department of Civil and Environmental Engineering, The Hong Kong Polytechnic University.
26. Ouyang W, Liu SW, Yang Y (2022) An improved morgenstern-price method using gaussian quadrature. *Comput Geotech* 148:104754
27. Qin C, Zhou J (2023) On the seismic stability of soil slopes containing dual weak layers: true failure load assessment by finite-element limit-analysis. *Acta Geotech* 18(6):3153–3175
28. Sarma SK (1973) Stability analysis of embankments and slopes. *Géotechnique* 23(3):423–433
29. Shi XS, Nie J, Zhao J, Gao Y (2020) A homogenization equation for the small strain stiffness of gap-graded granular materials. *Comput Geotech* 121:103440
30. Shi XS, Zhao J (2020) Practical estimation of compression behavior of clayey/silty sands using equivalent void-ratio concept. *J Geotech Geoenviron Eng* 146(6):04020046
31. Shi XS, Liu K, Yin JH (2021) Effect of initial density, particle shape, and confining stress on the critical state behavior of weathered gap-graded granular soils. *J Geotech Geoenviron Eng* 147(2):04020160
32. Shi XS, Liu K, Yin JH (2021) Analysis of mobilized stress ratio of gap-graded granular materials in direct shear state considering coarse fraction effect. *Acta Geotech* 16(6):1801–1814
33. Spencer E (1967) A method of analysis of the stability of embankments assuming parallel interslice forces. *Géotechnique* 17(1):11–26
34. Sun D, Wang L, Li L (2019) Stability of unsaturated soil slopes with cracks under steady-infiltration conditions. *Int J Geomech* 19(6):04019044
35. Wang HL, Cui YJ, Lamas-Lopez F, Dupla JC, Canou J, Calon N, Saussine G, Aïmedieu P, Chen RP (2018) Permanent deformation of track-bed materials at various inclusion contents under large number of loading cycles. *J Geotech Geoenviron Eng* 144(8):04018044
36. Wang HL, Cui YJ, Lamas-Lopez F, Dupla JC, Canou J, Calon N, Saussine G, Aïmedieu P, Chen RP (2017) Effects of inclusion contents on resilient modulus and damping ratio of unsaturated track-bed materials. *Can Geotech J* 54(12):1672–1681
37. Xiao T, Zhang LM, Cheung RWM, Lacasse S (2022) Predicting spatio-temporal man-made slope failures induced by rainfall in Hong Kong using machine learning techniques. *Géotechnique*, pp 1–17
38. Xie Q, Jie Y, Cui Y, Yin C (2023) Generating slip surfaces using the logistic function integral. *Int J Geomech* 23(5):04023034
39. Xiong X, Shi Z, Xiong Y et al (2019) Unsaturated slope stability around the Three Gorges Reservoir under various combinations of rainfall and water level fluctuation. *Eng Geol* 261(December 2018):105231
40. Xu DS, Yan JM, Liu Q (2021) Behavior of discrete fiber-reinforced sandy soil in large-scale simple shear tests. *Geosynth Int* 28(6):598–608
41. Xu DS, Huang M, Zhou Y (2020) One-dimensional compression behavior of calcareous sand and marine clay mixtures. *Int J Geomech* 20(9):04020137
42. Xu DS, Yin JH (2016) Analysis of excavation induced stress distributions of GFRP anchors in a soil slope using distributed fiber optic sensors. *Eng Geol* 213:55–63
43. Zhang F, Jia S, Shu S et al (2023) Stability charts for convex slope with turning arc. *Acta Geotech* 2:1–12
44. Zhang LL, Fredlund DG, Fredlund MD, Ward Wilson G (2014) Modeling the unsaturated soil zone in slope stability analysis. *Can Geotech J* 51(12):1384–1398
45. Zhang LL, Fredlund MD, Fredlund DG et al (2015) The influence of the unsaturated soil zone on 2-D and 3-D slope stability analyses. *Eng Geol* 193:374–383
46. Zhou J, Qin C (2022) Stability analysis of unsaturated soil slopes under reservoir drawdown and rainfall conditions: steady and transient state analysis. *Comput Geotech* 142:104541
47. Zhu DY, Lee CF, Qian QH et al (2001) A new procedure for computing the factor of safety using the Morgenstern-Price method. *Can Geotech J* 38(4):882–888
48. Zhu DY, Lee CF, Qian QH, Chen GR (2005) A concise algorithm for computing the factor of safety using the Morgenstern-Price method. *Can Geotech J* 42(1):272–278

**Publisher's Note** Springer Nature remains neutral with regard to jurisdictional claims in published maps and institutional affiliations.